A new high-pressure polymorph of phosphoric acid

Craig L. Bull, Nicholas P. Funnell, Colin R. Pulham, William G. Marshall and David R. Allan

Published version information

Citation: CL Bull et al. "A new high-pressure polymorph of phosphoric acid." Acta Crystallographica B, vol. 73, no. 6 (2017): 1068-1074.

DOI: 10.1107/S205252061701441X
.

Acta Cryst B
STRUCTURAL SCIENCE
CRYSTAL ENGINEERING
MATERIALS
ISSN 2052-5206

A new high-pressure polymorph of phosphoric acid

Craig L. Bull,[a] Nicholas P. Funnell,[a] Colin R. Pulham,[b] William G. Marshall[a]‡ and David R. Allan[c]*

[a]ISIS Facility, STFC Rutherford Appleton Laboratory, Harwell Science and Innovation Campus, Chilton, Didcot, Oxfordshire OX11 0QX, UK, [b]EaStCHEM School of Chemistry, Joseph Black Building, David Brewster Road, Edinburgh, EH9 3FJ, UK, and [c]Diamond Light Source Ltd, Diamond House, Harwell Science and Innovation Campus, Didcot, Oxfordshire, OX11 0DE, UK. *Correspondence e-mail: david.allan@diamond.ac.uk

Received 28 September 2017
Accepted 6 October 2017

Edited by A. Katrusiak, Adam Mickiewicz University, Poland

‡ 1963–2015

Keywords: high pressure; neutron powder diffraction; X-ray single-crystal diffraction; phosphoric acid; polymorph.

CCDC references: 1578418; 1578419; 1578420; 1578421; 1578422; 1578423; 1578424; 1578425; 1578426; 1578427; 1578428; 1578429; 1578430; 1578431; 1578432; 1578433; 1578434; 1578435; 1578436; 1578437; 1578438; 1578439; 1578440; 1578441; 1578442; 1578443; 1578444; 1578445; 1578446

Supporting information: this article has supporting information at journals.iucr.org/b

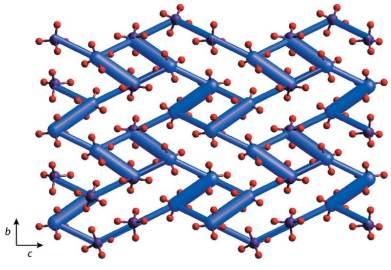

The high-pressure structural behaviour of phosphoric acid is described. A compression study of the monoclinic phase, using neutron powder diffraction and X-ray single-crystal diffraction, shows that it converts to a previously unobserved orthorhombic phase on decompression. Compression of this new phase is reported up to 6.3 GPa. The orthorhombic phase is found to be more efficiently packed, with reduced void space, resulting in a larger bulk modulus. Molecule–molecule interaction energies reveal a more extensive network of increased attractive forces in the orthorhombic form relative to the monoclinic form, suggesting greater thermodynamic stability.

1. Introduction

The mineral acids, or oxo-acids (H_xXO_y), nitric (HNO_3), sulfuric (H_2SO_4) and phosphoric (H_3PO_4) acids are ubiquitous compounds that find widespread application as bulk industrial compounds and as laboratory reagents (Thiemann *et al.*, 2000). For example, the manufacture of agricultural fertilizers accounts for most of the production of phosphoric acid (Schraüdter *et al.*, 2000). Several crystal structures have been determined for these mineral acids at low temperature and high pressure: nitric acid crystallizes in different $P2_1/c$ structures, either below 232 K (Luzzati, 1951) or above 1.6 GPa (Lucas & Petitet, 1999; Allan *et al.*, 2010) and sulfuric acid also has $P2_1/c$ symmetry at 0.7 GPa and a $C2/c$ form below 283 K (Allan *et al.*, 2002).

In general, the mineral acid crystal structures do not bear any strong likeness to each other, despite the fact they all have relatively simple molecular structures and interact predominantly *via* directional hydrogen bonding. At a molecular level, the sulfuric and phosphoric acids are the most similar. Each has a tetrahedral arrangement of O atoms around the central (S or P) atom and the acids are best formulated as $(OH)_2SO_2$ and $(HO)_3PO$, where the sulfuric acid molecule has two hydrogen bonds and the phosphoric acid molecule has three. The molecular and crystal structures of phosphoric acid are shown in Fig. 1.

In phase I, the phosphoric acid molecules crystallize in the space group $P2_1/c$ with $Z = 4$ and $Z' = 1$ (Blessing, 1988). The molecular packing along the *b* axis can be described as follows: neighbouring molecules are related by unit-cell translation and are connected by hydrogen bonds measuring 1.936 Å. Slabs of molecules (**c**/2 thick) are formed in the *ab* plane *via* 2_1 screw axes parallel to **b** (at $z = \frac{1}{4}$ and $\frac{3}{4}$) and these are held together by two sets of short, highly directional hydrogen

bonds (O···H measuring 1.560 and 1.572 Å) to molecules above and below the *ac* plane. Neighbouring slabs are stacked along **c**, repeating periodically every half-unit-cell translation. The neighbouring and innermost molecules of each slab are related by inversion centres (as are the outermost) and are held together by polar non-covalent interactions. The structure bears a slight resemblance to that of sulfuric acid at low temperature, as it too is composed of hydrogen-bonded layers of molecules (Kemnitz *et al.*, 1996; Sven, 1954, 1955; Smith *et al.*, 1955; Blessing, 1988), unlike the high-pressure phase of sulfuric acid where molecules arrange themselves into isolated chains (Allan *et al.*, 2002).

As part of an ongoing programme to explore the structural responses of the oxo-acids to pressure, we report the effects of compression on phosphoric acid, and present a new high-pressure orthorhombic crystal structure of phosphoric acid (hereinafter known as phase II). This new structure cannot be readily categorized as an easily recognisable assembly of structural elements such as layers, columns or ribbons, but instead the molecular arrangement suggests a more framework-like structure with a relatively complex hydrogen-bonding pattern. We have combined the techniques of neutron powder diffraction and single-crystal X-ray diffraction to determine accurately the atomic positions of this high-pressure phase, including those of the hydrogen atoms.

2. Experimental

2.1. High-pressure neutron powder diffraction

Perdeuterated phosphoric acid was prepared in accordance with the method of Greenwood & Thompson (1960). In brief, phosphorus pentoxide (99.999+% purity, Aldrich) was sublimed twice *in vacuo* in all-glass apparatus into a U-tube. A stoichiometric quantity of D_2O (Aldrich) was condensed into the U-tube and the resulting solution was then heated at 368 K for 24 h. The sample was then purified by repeated fractional crystallization under vacuum until a solid with a melting point of 319 K was obtained.

High-pressure time-of-flight neutron powder diffraction measurements were conducted on the PEARL high-pressure beamline located at the ISIS Facility, Rutherford Appleton Laboratory, UK (Bull *et al.*, 2016). The PEARL diffractometer is a high-flux, medium-resolution instrument optimized for data collection from a Paris–Edinburgh (P-E) pressure cell (Besson *et al.*, 1992). The phosphoric acid powder was loaded into a null-scattering Ti–Zr alloy capsule gasket (Marshall & Francis, 2002) at a temperature of ∼ 283 K, in a dry nitrogen atmosphere, to prevent loss of the volatile pentane pressure transmitting medium and condensation of hydrogenous water on the gasket and sample. The loaded gasket was then sealed within the P-E press equipped with standard toroidal profile zirconia-toughened alumina (ZTA) anvils which are highly neutron transparent, permitting increased data acquisition rates and improved quality (Bull *et al.*, 2016). In addition to the powdered sample, a small lead sphere (*circa* 0.8 mm diameter) and a mixture of deuterated pentanes were added to the gasket (Klotz *et al.*, 2009). In this standard setup, the lead acts as a suitable pressure calibration marker and the pentane mixture acts as a hydrostatic pressure-transmitting medium up to a pressure of ∼ 6 GPa (Klotz *et al.*, 2009). A series of diffraction patterns were collected with increasing hydrostatic pressure up to a maximum load of 48 tonnes (4.30 GPa) in approximately 3 tonne increments. The load was then reduced to 6 tonnes (2.0 GPa) where a phase transformation was observed. Further decompression to 2 tonnes resulted in a pressure of 0.9 GPa, after which the sample was recompressed in ∼ 3-tonne steps to a maximum pressure of 66 tonnes (6.26 GPa) and diffraction patterns were then obtained for the new high-pressure phase. During the experiment, the unit-cell volume of the Pb calibrant, as determined by Rietveld refinement, was used to determine the pressure from a previously determined Murnaghan equation of state (EoS) (Fortes *et al.*, 2007). Time-of-flight data were normalized and corrected using in-house software (Arnold *et al.*, 2014). A beamline-developed correction for the wavelength and scattering-angle dependence of the neutron attenuation by the ZTA anvils and Ti–Zr gasket materials was applied to the observed pattern (Bull *et al.*, 2016). *GSAS* and *EXPGUI* were used for Rietveld refinement (Toby, 2001). The scattering from the pressure calibrant and the anvil materials (alumina and tetragonal zirconia) was accounted for by additional crystalline phases in the Rietveld refinements. At loads beyond 10 tonnes (0.44 GPa) a contaminant phase of phosphoric acid hemihydrate was identified and included in all subsequent Rietveld refinements. Least-squares fits to the volume decrease with increasing pressure to determine the bulk

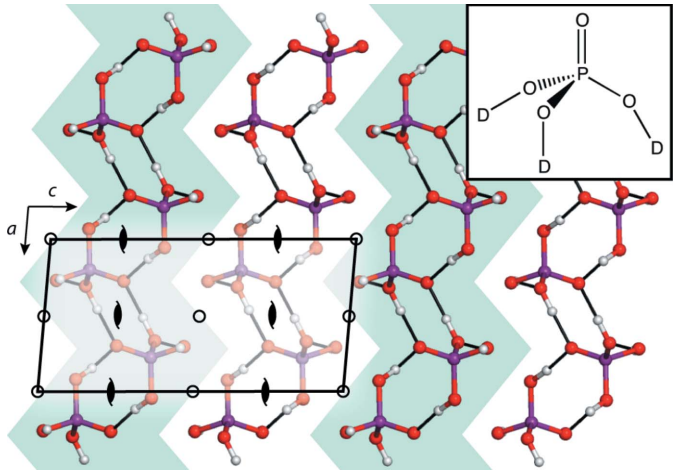

Figure 1
Monoclinic crystal structure of phosphoric acid (phase I) at 0.44 GPa (this study), viewed along the *b* axis. The molecular structure is shown in the inset in the top-right corner. Phosphorus atoms are shown in purple, oxygen atoms in red and hydrogen atoms in white. Hydrogen bonds are shown as black lines. Note, there are hydrogen bonds present along **b** that are obscured by the molecules in this orientation. The unit cell is indicated by the bordered translucent region, containing inversion centres (open circles) and 2_1 screw axes parallel to **b** ('pointed', filled ellipses). The green-shaded regions indicate alternating slabs of phosphoric acid molecules in the *ab* plane.

Table 1
Crystallographic data for the high-pressure studies of phosphoric acid.

X-ray experiments were carried out on a single-crystal sample and neutron experiments on powder. Dashes indicate that a value is not applicable or that data are not available.

Pressure (GPa)	0.50	1.80	0.01	4.30†	0.86	6.26
Radiation	X-ray	X-ray	Neutron	Neutron	Neutron	Neutron
Phase	I	II	I	I	II	II
Space group	$P2_1/c$	$P2_12_12_1$	$P2_1/c$	$P2_1/c$	$P2_12_12_1$	$P2_12_12_1$
a axis (Å)	5.707 (3)	4.619 (5)	5.7493 (5)	5.3264 (9)	4.6648 (4)	4.5121 (7)
b axis (Å)	4.820 (3)	8.479 (17)	4.8392 (3)	4.6618 (1)	8.6057 (7)	8.2009 (12)
c axis (Å)	11.436 (6)	14.38 (3)	11.6170 (8)	10.8294 (22)	14.5932 (11)	13.8569 (17)
β (°)	94.75 (7)	90	95.150 (7)	92.349 (19)	90	90
Volume (Å^3)	313.5 (3)	563.1 (17)	321.90 (3)	229.82 (6)	585.83 (5)	512.75 (7)
Density ρ (g cm^{-3})	2.076	2.312	2.084	2.373	2.291	2.617
Z'	1	2	1	1	2	2
No. of parameters‡	22	91	36	17	67	67
No. of reflections collected§	1255	2503	1768	1768	1840	1840
No. of unique reflections (R_{merge})	360 (0.086)	1649 (0.145)	–	–	–	–
No. of reflections [$I > 2\sigma(I)$]	294	1296	–	–	–	–
R_1 [$F^2 > 2\sigma(F^2)$] or R_{wp}	0.0720	0.1219	0.0457	0.0497	0.0445	0.0478
wR_2 (F^2, all data)	0.2169	0.3223	–	–	–	–
G.o.F.	0.982	1.104	1.323	2.459	1.74	1.14
$\Delta\rho_{max}$ (e Å^{-3})	0.45	1.23	–	–	–	–
$\Delta\rho_{min}$ (e Å^{-3})	−0.53	−1.26	–	–	–	–

† Refinement performed using LeBail extraction. ‡ For the neutron powder data the number of parameters relate only to the phosphoric acid phase and background, and not contaminant phases (from the anvils and pressure marker). § The number of reflections is across the d-spacing range 0.5–4.2 Å and include reflections from the anvils and pressure marker.

modulus were performed using the *EoS* suite of programmes (Gonzalez-Platas *et al.*, 2016).

2.2. High-pressure single-crystal X-ray diffraction

Phosphoric acid (of 99.999+% purity, as-received from Sigma–Aldrich) was loaded into a Merrill–Bassett diamond-anvil cell equipped with 600 µm culet diamonds and a pre-indented tungsten gasket (Merrill & Bassett, 1974). The loading was conducted under a dry nitrogen atmosphere and, as phosphoric acid is a solid at room temperature, the sample and the cell were heated to approximately 323 K after the diamond anvil cell was initially closed and sealed. An initial compression could then be conducted on the liquid phase. The sample was pressurized at this elevated temperature until the formation of several crystallites was observed. The temperature was then increased, so that the polycrystalline sample was partially melted, and subsequently cycled close to this elevated melting temperature in order to reduce the number of crystallites [in a manner similar to the methods of Vos *et al.* (1993)]. When only one crystallite remained, the cell was allowed to cool to room temperature and the resulting single crystal was observed to completely fill the sample chamber. The pressure was determined to be 0.5 (1) GPa using the ruby fluorescence technique (Mao *et al.*, 1986). The setting angles of 24 strong reflections were determined on an Enraf–Nonius CAD4 diffractometer (equipped with a Mo X-ray tube).

Intensity data were collected with the ω-scan method at the position of least attenuation by the pressure cell, according to the fixed φ-technique. All accessible reflections were measured in the shell $\pm h, \pm k, \pm l$ for $0 < \sin\theta/\lambda < 0.48$ Å^{-1}. The intensities were corrected for absorption by the diamond anvil cell and then used for structure solution by direct methods (*SHELX*97; Sheldrick, 2008) in $P2_1/c$ symmetry. One molecule was identified in the asymmetric unit (*i.e.* $Z' = 1$) and the structure subsequently refined against F^2 (*SHELX*97; Sheldrick, 2008). The hydrogen atoms were located by geometric placement and refined using geometric constraints. All hydrogen atoms were constrained such that U_{iso}(H) values were equal to $1.2 \times U_{eq}$ of their respective parent atoms. The refinement statistics of the final fit are listed in Table 1. The pressure was then increased to ~ 2 GPa and the sample recrystallized using the aforementioned technique and data collected again in the manner described above.

2.3. Analytical procedures

Interstitial void calculations were carried out in *Mercury*3.9 (Macrae *et al.*, 2008) using the minimum available values for probe radius and grid spacing −0.2 and 0.1 Å, respectively. Dispersion-corrected interaction energies were calculated between molecules within a 3.8 Å radius, at the B3LYP-D2 6-31G(d,p) level, using the *Tonto* package implemented in *CrystalExplorer*17 (Turner *et al.*, 2017, 2014). The same program was used to display these energies as frameworks, using a common scale factor to allow direct comparison between the images produced (Turner *et al.*, 2015).

3. Results

3.1. Neutron powder diffraction of phases I and II

Fig. 2 shows the diffraction patterns of the known monoclinic phase I and its associated Rietveld refinement at a pressure of ~ 0.01 GPa and is described in the figure caption. The structure is almost identical to that determined by Blessing (1988) at low temperature. The quality of data was such

that consistent results could only be obtained with the aid of suitable geometric restraints being applied to the GSAS structure refinements. The restraint values used were based on the corresponding bond lengths and angles given in the phase-I structure determination by Blessing and were as follows: d(P—O) = 1.55 (2) Å, d(P═O) = 1.50 (5) Å, d(O—D) = 0.95 (5) Å and ∠(O—P—O′) = 109.5 (30)°, *i.e.* the PO_4 group is close to an ideal tetrahedron. The load on the sample was sequentially increased and the variation in diffraction pattern is shown in the supporting information. Fig. 3 shows the variation in the molar volume of phase I as a function of pressure. The fitted EoS is shown in the same figure as a solid line and was obtained by a least squares fit to a third-order Birch–Murnaghan isothermal EoS; the fitted values are V_0 = 322.01 (10) Å^3, B_0 = 13.81 (15) GPa, B' = 5.75 (15). The highest pressure measured for phase I was 4.30 GPa (LeBail extraction only possible for this data set). However, it was not possible to go beyond this pressure owing to experimental time constraints. To this end the pressure was reduced and, at an applied load of 6 tonnes, a phase transition was observed; the sample pressure was determined to be 1.97 GPa. This transformation is shown sequentially in Fig. 4. This phase, which we have called phase II, had not been observed previously and it was impossible to index the diffraction pattern definitively as a result of the relatively narrow range of d-spacing available on the PEARL instrument. Following a

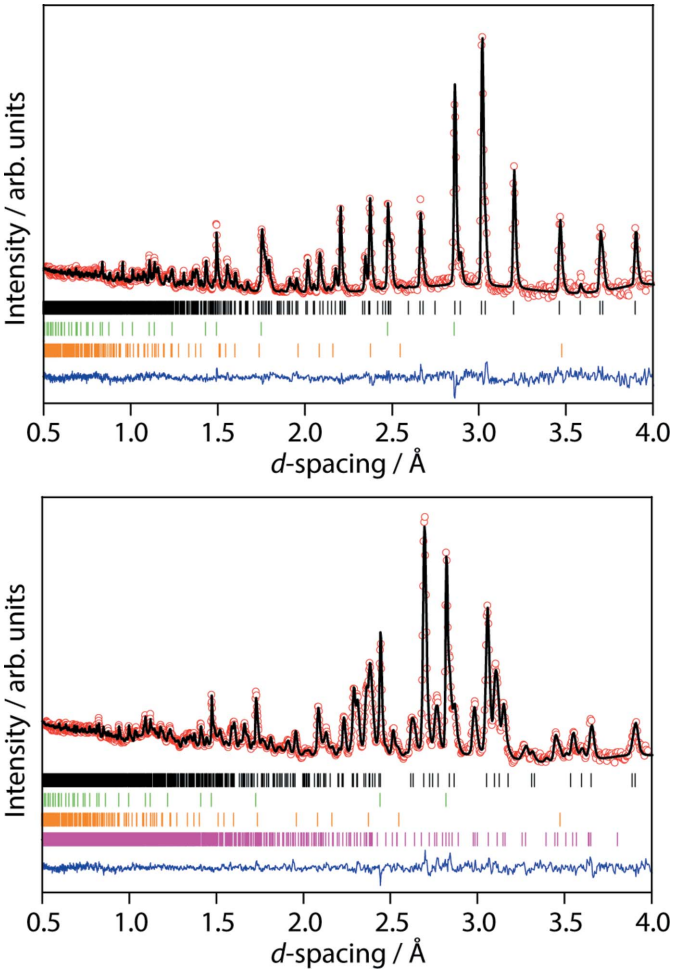

Figure 2
Neutron diffraction patterns and Rietveld fits to data for (top) monoclinic phase I and (bottom) orthorhombic phase II, at 0.01 and 1.97 GPa, respectively. In both plots the observed data are shown as open red circles, the solid black trace shows the calculated profile and the bottom blue trace shows the residual of the fit. The tick marks show the expected reflection positions for each of the phases fitted in the patterns, which are, from top to bottom, D_3PO_4 (black), Pb (green), Al_2O_3 (orange), and at higher pressures a phosphoric acid hemihydrate contaminant phase was also observed (purple tick marks).

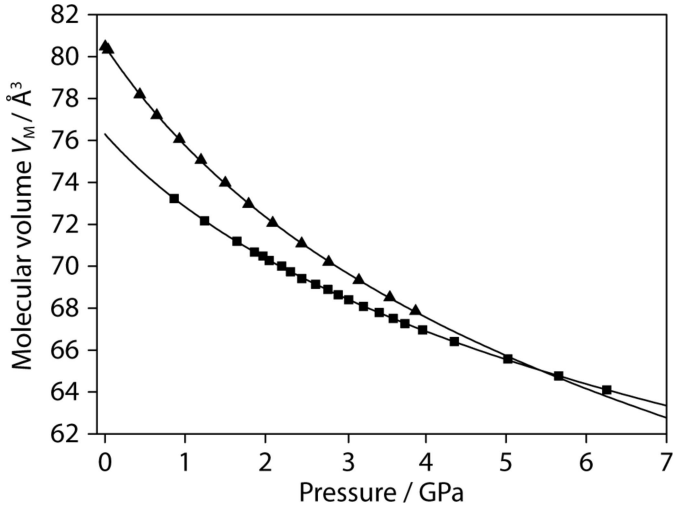

Figure 3
Variation in fitted molecular volume of phase I (triangles) and phase II (squares). A fitted third-order Birch–Murnaghan isothermal EoS is shown for both phases with a solid line. The fits yield values of V_0 = 322.0 (1) Å^3, B_0 = 13.81 (15) GPa, B' = 5.75 (15) for phase I (with Z = 4) and V_0 = 610.4 (4), B_0 = 17.6 (4), B' = 8.8 (2) for phase II (Z = 8). Error bar are smaller than the symbols.

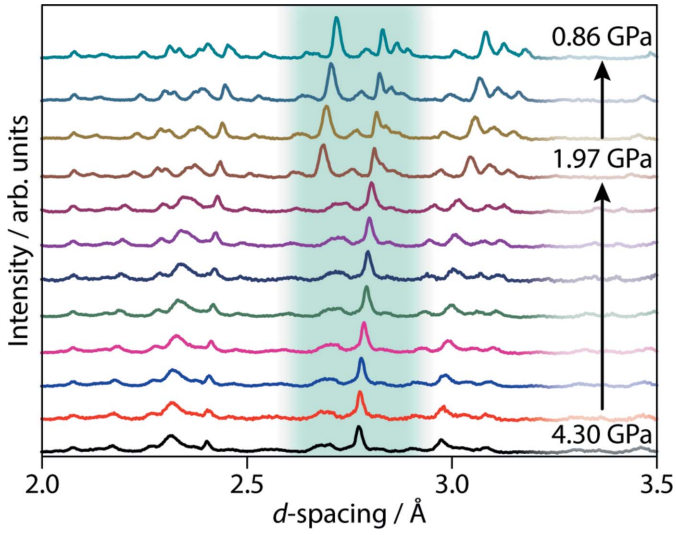

Figure 4
Variation in the neutron diffraction pattern of phosphoric acid on downloading from 4.30 GPa to 0.86 GPa. Upon downloading, a transformation is detected in the diffraction pattern at ∼ 1.97 GPa. Clear changes are observed at ∼ 2.75 and 2.85 Å (shaded region) and the resulting pattern can only be indexed as orthorhombic phase II. Equivalent plots for the initial compression of phase I, and re-compression of the newly transformed phase II are given in the supporting information.

further decompression to 2 tonnes (0.9 GPa), this phase was re-compressed in steps of ∼3 tonnes up to a maximum applied load of 66 tonnes, resulting in a sample pressure of 6.26 GPa, which is the upper limit of the accessible hydrostatic regime of pentanes. The sample was then recovered back to ambient pressure at which point it reverted to the monoclinic phase, I.

3.2. X-ray single-crystal study

As the structure of phase II was unknown, a high-pressure single-crystal study was undertaken to allow indexing and a potential structure to be determined. This could then be used as a starting model for the previously collected neutron powder diffraction data. As noted earlier, a single-crystal data set was initially obtained from a sample in the known phase-I structure. Refinement of the data set confirmed the monoclinic symmetry as previously reported by Blessing (1988). A single crystal grown from the melt at higher pressure could not be indexed using the monoclinic phase I unit cell, but instead was found to be orthorhombic with a = 4.619 (5) Å, b = 8.479 (17) Å, c = 14.38 (3) Å and V = 563.1 (17) Å^3 at 1.8 (1) GPa. Intensity data were collected using an identical data collection strategy as for phase I and the structure was solved with $P2_12_12_1$ symmetry using direct methods (*SHELX*97; Sheldrick, 2008). Two molecules were identified in the asymmetric unit (Z' = 2) and, as before, the structure was refined against F^2 using *SHELX*97 (Sheldrick, 2008). The hydrogen atom positions were located by identifying possible oxygen–oxygen hydrogen-bond host atom distances and they were refined using geometrical constraints. Treatment of the hydrogen atomic displacement parameters was identical to that of phase I. The statistics of the converged refinement are listed in Table 1. Atomic coordinates are available in CIF format in the supporting information.

3.3. Processing the neutron powder data of phase II

Following determination of a potential structure for phase II by single-crystal X-ray diffraction, the neutron powder diffraction patterns of the new phase were indexed using the orthorhombic structure, which accounted for all observed reflections. Rietveld analysis used the coordinates of the phosphorus and oxygen atoms from the single-crystal refinement as starting positions and were subsequently allowed to refine. The positions of the deuterium atoms in the phase-II structure were inferred using geometrical and hydrogen-bonding considerations for the structural refinements using the X-ray data. These positions were tested and confirmed by the neutron powder diffraction data by means of a sequence of refinement cycles which located each deuterium atom in turn using Fourier difference maps; after removing the deuterium atoms, the first Fourier cycle revealed the coordinates of the first deuterium atom and each further cycle located an additional deuterium atom. Details of the structure are given in the supporting information and representative Rietveld fits to the data are shown in Fig. 2. Again, suitable restraints were used to ensure realistic bond distances as described in §3.1. With the structure and symmetry known, it was possible to fit all data sets collected in phase II; the variation in unit-cell volume is shown in Fig. 3. The fitted EoS is shown as the solid line and was obtained by a least-squares fit to a third-order Birch–Murnaghan isothermal EoS; the fitted values are V_0 = 610.4 (4) Å^3, B_0 = 17.61 (36) GPa and B' = 8.76 (23). Phase II reverted to phase I on decompression to ambient conditions.

3.4. The crystal structure of phase II

The phase-II structure, shown in Fig. 5, is an orthorhombic cell ($P2_12_12_1$) containing eight molecules, which is twice as many as phase I. Similar to phase I, there are alternating layers of molecules across the unit cell – now in the *ab* plane – but these are now only **c**/4 thick and are symmetry-independent of their neighbouring layers (indicated by their differing colours in the figure), as a result of there being a second molecule in the asymmetric unit. The molecules within the first layer (numbered '1' in Fig. 5), are related to their neighbours along **a** by periodic translation and along **b** by 2_1 screw axes parallel to **a**. In the second layer ('2'), the molecules are translated in **c**, and are offset in the *ab* plane by a quarter translation along both axes. Neighbouring molecules within layer 2 are related by 2_1 screw axes aligned with **b**. The first and second layers are related to the third and fourth, respectively, by 2_1 axes parallel to the *a* and *c* axes. Each layer is connected to its neighbour *via* a relatively complex set of H(D)-bonding interactions, with no easily-described pattern, with D···O distances ranging between 1.57 and 1.99 Å at 0.86 GPa. Atomic coordinates are available in CIF format in the supporting information.

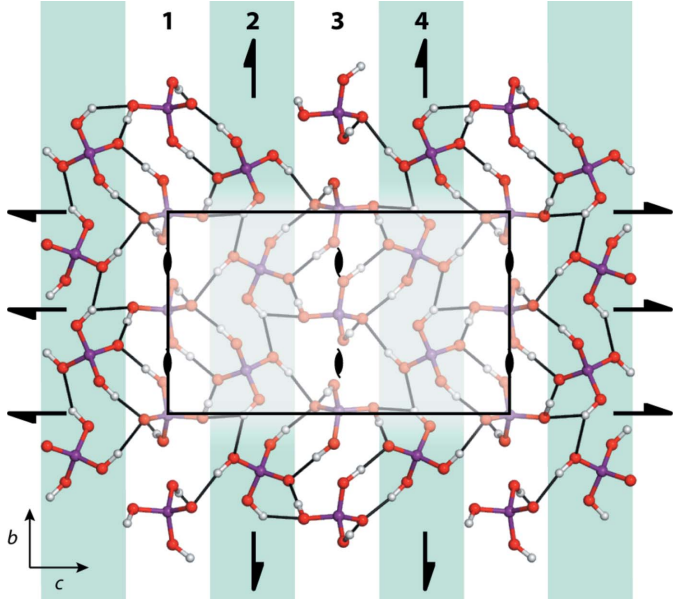

Figure 5
Crystal structure of phase II at 0.86 GPa. The half-headed arrows indicate the 2_1 screw axes along **b** and **c**. The numbering of the layers, referred to in the main text, is given at the top of the figure. Here, the green and white areas indicate molecules related by symmetry.

4. Discussion

4.1. Compressibility of phosphoric acid

The two high-pressure structures of phosphoric acid obtained in this study do not bear any obvious geometric relationship to each other, so we have explored the structures as observed from the viewpoint of each molecule in the asymmetric units. Hirshfeld fingerprint plots, which are a graphical representation of contact distances within the crystal, provide an insight into changes in the local environment of each crystallographically unique molecule, see Fig. 6. For a more thorough explanation of Hirshfeld surfaces and their corresponding fingerprint plots, the reader is referred to Spackman & Byrom (1997), but in brief, each fingerprint plot is unique to a given molecule and its features can be attributed to particular motifs in the crystal, notably the 'spiky' regions at shorter d_e and d_i distances (shortest distance to nuclei on the exterior and interior of the Hirshfeld surface, respectively) depict hydrogen bonding. Despite the very different packing between phases I and II, the fingerprint plots indicate only quite subtle changes in hydrogen-bonding distances, a feature also seen in nitric acid [see Figure 8 in paper by Allan *et al.* (2010)]. More apparent is the decrease in distance of the centre of gravity of the fingerprint, suggesting a more efficient packing of phosphoric acid molecules overall, rather than decreasing intermolecular bonding distances. This is consistent with a decrease in the calculated void space in each unit cell. A comparison of the two structures at similar pressures shows that phase II is always the more efficiently packed; 20.6% of the unit-cell volume in phase I at 0.93 GPa comprises interstitial voids, compared with 16.8% in phase II at 0.86 GPa. This difference in packing is observed across the whole pressure range for which we have structural data (see Fig. S4 in the supporting information). Extrapolation to higher pressures suggests that by ~ 5.5 GPa, phase I should be the more efficiently packed (see Fig. 3) but, regrettably, diffraction data for phase I are not available at this pressure. Previous high-pressure studies on molecular systems have shown that the space between molecules is compressed, in preference to molecules themselves, and this is a probable explanation for the larger bulk modulus observed for phase II.

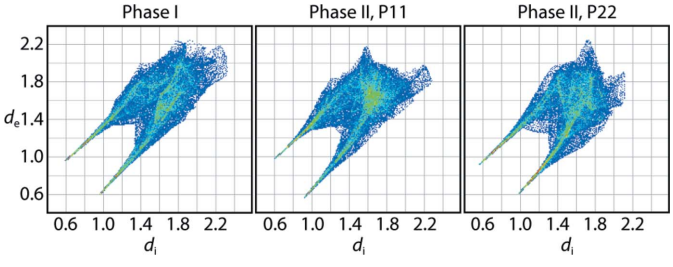

Figure 6
Hirshfeld fingerprint plots for the unique molecules in phases I and II. 'P11' and 'P22' refer to the numbering used for the unique phosphorous atoms in the structure refinements (see the CIF in the supporting information). Closest nuclei distances exterior (d_e) and interior (d_i) to the Hirshfeld surface are given in ångströms.

4.2. Energy frameworks

The strength of bonding interactions in molecular crystals is often judged on the distance and directionality of hydrogen bonding, where there are suitable acceptor and donor atoms present. Although the assumption is often made that a short hydrogen bond must be a favourable bonding interaction (and is frequently true), there are known examples where this is misleading and they are actually net destabilizing forces that are being counterbalanced by other favourable interactions (*e.g.* long-range electrostatic attraction) (Moggach *et al.*, 2015). In this case, phase I is easily described in terms of its hydrogen-bonding network, but in phase II this is not so straightforward; earlier we described this phase as being more 'framework-like'. It is instructive to look at the structures as represented by a network of calculated relative energies [this is available with the 'energy framework' option in *CrystalExplorer*, where interaction energies calculated at the B3LYP-D2 6-31G(d,p) level can be visualized as cylinders between molecular centroids, the radii of which are proportional to the interaction magnitude]. The total energies presented are the sum of individual electrostatic, polarization, repulsion and dispersion terms, thus in general, net stabilizing forces are shown (with blue cylinders, see Fig. 7). We do not intend to use these to provide a rigorous quantitative description of interactions energies here, but they are informative for a qualitative understanding of the general distribution of stabilizing and destabilizing forces across the unit cell.

In phase I, the hydrogen-bonding network does in fact map quite closely onto that of the attractive forces, the latter shown in Fig. 7, left column (compare with the hydrogen bonding in Fig. 1). The energy frameworks are more revealing for phase II, where it becomes obvious that the molecules are stabilized as pairs of dimers, *i.e.* four molecules (see Fig. 7, upper right

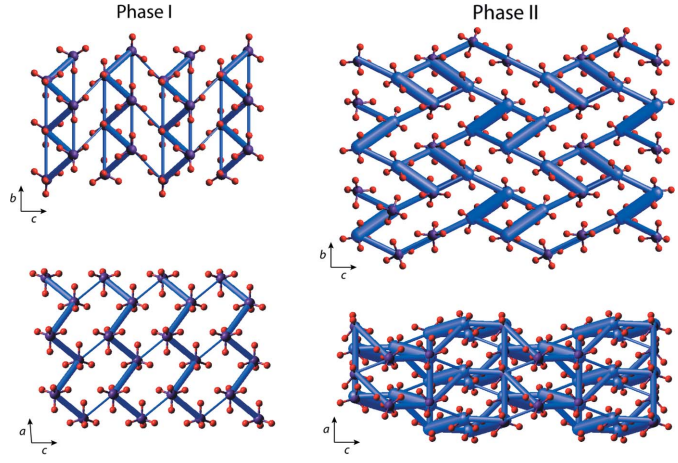

Figure 7
Energy frameworks for phase I (left column) ad phase II (right column). The upper and lower rows show projections along **a** and **b**, respectively. Note there is no crystallographic equivalence between the monoclinic and orthorhombic cells along the same direction. Hydrogen atoms are omitted for clarity and all structures are shown on the same scale. The total, stabilizing, intermolecular energy is shown with blue cylinders. Interactions below 15 kJ mol^{-1} are not shown in order to highlight the strongest forces.

panel), between which the strongest interactions are located, lying in the *bc* plane. Each set of dimers is located directly above and below an equivalent set of pairs, such that columnar stacks are formed along **a** (see Fig. 7, lower right panel). Neighbouring columns, offset by a half-cell translation in **a**, are anchored to each other *via* an interaction approximately half the strength of those within the dimers. The size of the cylinders is directly comparable between the two phases and shows that the strength of the intermolecular interactions generally increases on going from phase I to phase II.

It is also notable that the 'dimensionality' of the attractive force network increases in the I → II transition. The majority of attractive energies in phase I are aligned within slabs of molecules in the *ab* plane, but these are stacked along the *c* direction where there are few strong interactions; in this sense, the energy framework is somewhat 'two dimensional', where we might expect the stacking axis to align with the most compressible direction. However, it is the *a* axis that changes the most over the course of compression, decreasing by 7.13% of its original length, compared with 6.48% in **c**. We note that it would be more common to discuss the variation in the compression of the orthogonal strain tensor axes; however, the compression in this material occurs as changes in the packing of slabs within the structure. Inspection of the crystal structure reveals that the largest voids lie between molecules along the *a* axis, making this the preferred direction of compression.

In phase II, there are relatively strong interactions in all three dimensions, which may further explain the larger bulk modulus of phase II. A comparison of the orthogonal cell axes, which are now coincident with the strain tensor, show that over the course of compression **a**, **b** and **c** change by 2.35, 3.30, and 3.69%, respectively. This decrease in compressibility (relative to phase I) is consistent with the development of stronger interactions overall, with generally three-dimensional connectivity.

5. Conclusions

We have observed a new orthorhombic phase of phosphoric acid which, at high pressure, appears to be the thermodynamically stable phase, and as it reverts back to phase I upon decompression, is less thermodynamically favourable at ambient pressure. There is a distinct difference in their compressibilities and this is a result of the difference in the relative molecule unit alignments. In phase II there are strong interactions in all three dimensions, resulting in a stiffer material, in contrast to phase I where the majority of strong interactions are only in the *ab* plane and not along the *c* direction (resulting in different amounts of void space in the two structures). Both phases of phosphoric acid show very few structural similarities to the known phases of the other mineral acids.

Acknowledgements

The work has been supported by facilities made available by STFC. The authors wish to thank Chris Goodway for assistance with the neutron experiments and Pam McGregor for assistance in collecting the single-crystal data. Lastly, we acknowledge the efforts of our late colleague William 'Bill' Marshall who contributed much towards the data collection and processing reported in this manuscript.

Funding information

The work has been supported by an EPSRC grant.

References

Allan, D. R., Clark, S. J., Dawson, A., McGregor, P. A. & Parsons, S. (2002). *J. Chem. Soc. Dalton Trans.* pp. 1867–1871.
Allan, D. R., Marshall, W. G., Francis, D. J., Oswald, I. D. H., Pulham, C. R. & Spanswick, C. (2010). *Dalton Trans.* **39**, 3736–3743.
Arnold, O. *et al.* (2014). *Nucl. Instrum. Methods Phys. Res. A*, **764**, 156–166.
Besson, J. M., Nelmes, R. J., Hamel, G., Loveday, J. S., Weill, G. & Hull, S. (1992). *Physica B*, **180–181**, 907–910.
Blessing, R. H. (1988). *Acta Cryst.* B**44**, 334–340.
Bull, C. L., Funnell, N. P., Tucker, M. G., Hull, S., Francis, D. J. & Marshall, W. G. (2016). *High Press. Res.* **36**, 493–511.
Fortes, A. D., Wood, I. G., Alfredsson, M., Vočadlo, L., Knight, K. S., Marshall, W. G., Tucker, M. G. & Fernandez-Alonso, F. (2007). *High Pressure Res.* **27**, 201–212.
Gonzalez-Platas, J., Alvaro, M., Nestola, F. & Angel, R. (2016). *J. Appl. Cryst.* **49**, 1377–1382.
Greenwood, N. N. & Thompson, A. (1960). *Inorg. Synth.* **7**, 81–84.
Kemnitz, E., Werner, C. & Trojanov, S. (1996). *Acta Cryst.* C**52**, 2665–2668.
Klotz, S., Chervin, J. C., Munsch, P. & Le Marchand, G. (2009). *J. Phys. D Appl. Phys.* **42**, 075413.
Lucas, H. & Petitet, J.-P. (1999). *J. Phys. Chem. A*, **103**, 8952–8958.
Luzzati, V. (1951). *Acta Cryst.* **4**, 120–131.
Macrae, C. F., Bruno, I. J., Chisholm, J. A., Edgington, P. R., McCabe, P., Pidcock, E., Rodriguez-Monge, L., Taylor, R., van de Streek, J. & Wood, P. A. (2008). *J. Appl. Cryst.* **41**, 466–470.
Mao, H.-K., Xu, J. & Bell, P. M. (1986). *J. Geophys. Res.* **91**, 4673.
Marshall, W. G. & Francis, D. J. (2002). *J. Appl. Cryst.* **35**, 122–125.
Merrill, L. & Bassett, W. A. (1974). *Rev. Sci. Instrum.* **45**, 290–294.
Moggach, S. A., Marshall, W. G., Rogers, D. M. & Parsons, S. (2015). *CrystEngComm*, **17**, 5315–5328.
Schraüdter, K., Bettermann, G., Staffel, T., Wahl, F., Klein, T. & Hofmann, T. (2000). *Phosphoric Acid and Phosphates.* Wiley-VCH Verlag GmbH and Co. KGaA.
Sheldrick, G. M. (2008). *Acta Cryst.* A**64**, 112–122.
Smith, J. P., Brown, W. E. & Lehr, J. R. (1955). *J. Am. Chem. Soc.* **77**, 2728–2730.
Spackman, M. A. & Byrom, P. G. (1997). *Chem. Phys. Lett.* **267**, 215–220.
Sven, F. (1954). *Acta Chem. Scand.* p. 532.
Sven, F. (1955). *Acta Chem. Scand.* pp. 1557–1566.
Thiemann, M., Scheibler, E. & Wiegand, K. W. (2000). *Nitric Acid, Nitrous Acid, and Nitrogen Oxides.* Wiley-VCH Verlag GmbH and Co. KGaA.
Toby, B. H. (2001). *J. Appl. Cryst.* **34**, 210–213.
Turner, M. J., Grabowsky, S., Jayatilaka, D. & Spackman, M. A. (2014). *J. Phys. Chem. Lett.* **5**, 4249–4255.
Turner, M., McKinnon, J., Wolff, S., Grimwood, D., Spackman, P. D. J. & Spackman, M. (2017). *CrystalExplorer*17. University of Western Australia.
Turner, M. J., Thomas, S. P., Shi, M. W., Jayatilaka, D. & Spackman, M. A. (2015). *Chem. Commun.* **51**, 3735–3738.
Vos, W. L., Finger, L. W., Hemley, R. J. & Mao, H.-K. (1993). *Phys. Rev. Lett.* **71**, 3150–3153.